

# The novel role of circular RNA ST3GAL6 on blocking gastric cancer malignant behaviors through autophagy regulated by the FOXP2/MET/mTOR axis

**Penghui Xu**

The First Affiliated Hospital of Nanjing Medical University

**Xing Zhang**

The First Affiliated Hospital of Nanjing Medical University

**Jiacheng Cao**

The First Affiliated Hospital of Nanjing Medical University

**Jing Yang**

The First Affiliated Hospital of Nanjing Medical University

**Zetian Chen**

The First Affiliated Hospital of Nanjing Medical University

**Weizhi Wang**

The First Affiliated Hospital of Nanjing Medical University

**Sen Wang**

The First Affiliated Hospital of Nanjing Medical University

**Lu Zhang**

The First Affiliated Hospital of Nanjing Medical University

**Li Xie**

The First Affiliated Hospital of Nanjing Medical University

**Lang Fang**

The First Affiliated Hospital of Nanjing Medical University

**Yiwen Xia**

The First Affiliated Hospital of Nanjing Medical University

**Zhe Xuan**

The First Affiliated Hospital of Nanjing Medical University

**Jialun Lv**

The First Affiliated Hospital of Nanjing Medical University

**Zekuan Xu** (✉ [xuzekuan1@126.com](mailto:xuzekuan1@126.com))

Department of General Surgery, The First Affiliated Hospital of Nanjing Medical University, Nanjing, 210029.  
Jiangsu province, China

---

**Research Article**

**Keywords:** circST3GAL6, FOXP2, transcription factor, gastric cancer, autophagy

**Posted Date:** August 17th, 2021

**DOI:** <https://doi.org/10.21203/rs.3.rs-402505/v3>

**License:**   This work is licensed under a Creative Commons Attribution 4.0 International License. [Read Full License](#)

---

# Abstract

Gastric cancer (GC) ranks third in mortality among all cancers worldwide. Circular RNAs (circRNAs) play essential roles in the malignant progression and metastasis of gastric cancer. As a transcription factor, FOXP2 is involved in the progression of many tumours. However, the regulation and association between circRNAs and FOXP2 remain to be discovered. In our study, CircST3GAL6 was significantly depressed in GC tissues and cells. circST3GAL6 overexpression inhibited the proliferation, invasion and metastasis of GC cells in vitro and in vivo. Importantly, circST3GAL6 overexpression induced apoptosis and promote autophagy in GC cells. Furthermore, we found that circST3GAL6 sponged miR-300 and subsequently regulated FOXP2. We further revealed that FOXP2 suppressed the activation of the Met/AKT/mTOR axis, a classic pathway that regulates autophagy-mediated proliferation and migration. In summary, our findings revealed that circST3GAL6 functions as a tumour suppressor through the miR-300/FOXP2 axis in GC, regulates apoptosis and autophagy through FOXP2-mediated transcriptional inhibition of the MET axis and may be a biomarker for GC treatment.

## Introduction

Gastric cancer (GC) is the third most frequent cause of cancer-related deaths worldwide. According to the Global Cancer Statistics published in the *American Journal of Clinical Oncology* in 2018, GC ranks fifth in incidence and third in mortality among all cancers. East Asia, including China, has a high incidence of gastric cancer<sup>1,2</sup>. Although much progress has been made in improving the quality of life of gastric cancer patients<sup>3-5</sup>, the overall survival of GC patients has remained unsatisfactory in recent years<sup>6</sup>. Therefore, it is valuable to explore the potential mechanism and identify possible clinical therapeutic targets.

As noncoding RNAs, circular RNAs (circRNAs) are formed in a covalently circular closed loop, with a 3' head binding to 5' tail ends<sup>7</sup>. CircRNAs have been detected in many organisms and have become a hot topic of research in recent years because of their unique stable structure<sup>8,9</sup>. Furthermore, circRNAs have been reported to play many important roles in regulating translation, sponging miRNA and proteins<sup>10-12</sup>. Increasing evidence has confirmed that circRNAs function in GC development by sponging miRNAs to regulate targeted genes<sup>13</sup>. For example, the circular RNA circ-ERBIN promotes the growth and metastasis of colorectal cancer by miR-125a-5p and miR-138-5p/4EBP-1-mediated cap-independent HIF-1 $\alpha$  translation<sup>14</sup>. In the present study, we attempted to elucidate the molecular mechanisms of the suppressive role of circST3GAL6 in gastric cancer.

As a transcription factor, the Forkhead box P (FOXP) family comprises FOXP1, FOXP2, FOXP3 and FOXP4. FOXP proteins play essential roles in the regulation of gene transcription related to tumour progression<sup>15</sup>. Although FOXP3 is a well-known transcription factor, FOXP2 has rarely been investigated<sup>16,17</sup>. Recent studies have demonstrated that FOXP2 markedly affects cancer progression as a tumour suppressor<sup>18</sup>. For example, FOXP2 suppressed the transcriptional activity of MET, and FOXP2 overexpression resulted in the transcriptional repression of MET<sup>19</sup>. However, no relevant study has investigated the association between circRNAs and FOXP2, and how FOXP2 is regulated by circRNAs remains to be solved.

Autophagy is essential to tumour progression, and several studies have indicated that circRNAs are involved in the regulation of autophagy in cancer<sup>10,20</sup>. Additionally, the Met/mTOR axis regulates autophagy

and promotes tumour metastasis<sup>21</sup>.

In our study, we found that circST3GAL6 is downregulated in GC tissues. Furthermore, we demonstrated that circST3GAL6 suppresses cell proliferation and metastasis by sponging miR-300, affecting FOXP2 expression. CircST3GAL6 also regulates autophagy-mediated proliferation and migration through the FOXP2/Met/mTOR axis. In conclusion, circST3GAL6 is expected to be a therapeutic target in the future.

## Materials And Methods

### Tissue specimens/Tissue samples

All GC tissues and adjacent normal stomach mucosa tissues in this study were obtained from patients who had received radical gastrectomy at the Department of Gastrointestinal Surgery, the First Affiliated Hospital of Nanjing Medical University. All the specimens were collected and snap-frozen in liquid nitrogen immediately after surgical resection. TNM stage was based on the TNM classification system (American Joint Committee on Cancer classification, AJCC, 7<sup>th</sup> edition).

### Cell culture and treatment

The human GC cell lines BGC-823, SGC-7901, MGC-803, and MKN-45 and normal GES-1 stomach mucosa epithelium cells were cultured in RPMI 1640 (Wisent, Shanghai, China) supplemented with 10% foetal bovine serum (FBS) (Wisent, Biocenter, China) and 1% penicillin-streptomycin. HGC-27 cells were cultured in RPMI 1640 (Wisent, Shanghai, China) supplemented with 20% FBS (Wisent, Biocenter, China) and 1% penicillin-streptomycin. All the cells were incubated in a humidified atmosphere of 5% CO<sub>2</sub> at 37 °C.

### RNA-seq analysis

Total RNA was isolated from GC tissues and cells using TRIzol reagent (Invitrogen). Next, complementary DNA (cDNA) was reverse transcribed using PrimeScript RT Reagent (RR036A; TaKaRa, Japan). Quantitative real-time polymerase chain reaction (qRT-PCR) was performed using the SYBR™ GREEN PCR Master Mix kit (4913914001; Roche, Shanghai, China). The relative expression of RNA was normalized to the endogenous control glyceraldehyde 3-phosphate dehydrogenase (GAPDH) and U6. RIBOBIO Biotech (Guangzhou, China) provided all the specific primers for circRNAs. The PCR primer sequences of miRNAs and mRNAs were synthesized by Realgene (Nanjing, China) and are listed in Additional file 1: Table S1.

### RNase R treatment

The total RNA of GC cell lines was mixed with 3 U/mg of RNase R for 20 min at 37 °C. qRT-PCR was applied to detect the stable expression of circST3GAL6 and ST3GAL6 mRNA.

### Actinomycin D assay

Cells were seeded at 5×10<sup>4</sup> cells per well in a 24-well plate overnight and then treated with 2 mg/L of actinomycin D (Sigma-Aldrich, USA). Total RNA was harvested at the indicated time points (4 h, 8 h, 12 h, 24 h), and qRT-PCR was performed to analyse the stability of the circRNA and mRNA.

## **Oligonucleotide transfection**

The human gastric cell lines BGC-823 and SGC-7901 were seeded in a 6-well plate and incubated at 37 °C in a humidified 5% CO<sub>2</sub> atmosphere overnight. siRNA, miRNA mimics and inhibitors (GenePharma, Shanghai, China) were transfected with Lipofectamine 3000 (Thermo Fisher, Scientific, Waltham, MA, USA) according to the manufacturer's protocol.

## **Plasmid construction and stable transfection**

CircST3GAL6 cDNA was synthesized and cloned into the pcDNA3.1 vector (GenePharma, Shanghai, China). Cells were transfected with plasmids according to the manufacturer's protocol.

## **Western blotting**

Total protein from tissues and cells was extracted using RIPA lysis buffer (P0013B; Beyotime Biotechnology, China) containing PMSF. The protein concentration was determined using the Bradford method. Equal amounts of protein samples were resolved and separated by 10% SDS-PAGE using an electrophoresis apparatus (Bio-Rad, America) and transferred onto polyvinylidene difluoride (PVDF) membranes. Next, the membranes were blocked by incubating with Quick Block (P0252; Beyotime Biotechnology, China) for 20 minutes. Next, the membranes were treated with primary antibody, using GAPDH as an internal reference, at 4°C overnight. Finally, the membranes were washed and then incubated with secondary antibody for 2 h at room temperature. The blots were then visualized by enhanced chemiluminescence detection.

## **CCK-8 assay**

We plated BGC-823 and SGC-7901 cells in 96-well plates at ten thousand cells per well, and then added 10 µl of CCK-8 solution (Dojindo Laboratories, Kumamoto, Japan) to each well every other day according to the manufacturer's protocols. After that, the cells were cultured for 2 hours at 37°C. Two hours later, we recorded the absorbance of the cells at 450 nm using a microplate reader (BioTek, Winooski, VT, USA).

## **Colony formation assay**

BGC-832 and SGC-7901 cells were seeded in different six-well plates. Each well was inoculated with 1000 cells, and then the six-well plates were cultured in an incubator containing 5% CO<sub>2</sub> for 2 weeks. Two weeks later, the cell proliferation state was observed after staining the cells.

## **Transwell assay**

First, we inoculated specific cells on the upper side of the Transwell compartments (Millipore, Billerica, MA, USA) and added 200 µl serum-free RPMI-1640 at the same time. Next, we added 600µl of complete medium to the lower side of the Transwell compartments. After incubation for 24 hours in an incubator containing 5% CO<sub>2</sub>, we rinsed the cells with PBS and then removed the cells that did not pass through the membrane with a cotton swab. Finally, we fixed and stained the cells with 75% alcohol and crystal violet.

## **Flow cytometric analysis**

First, we inoculated the transfected cells in six-well plates. Next, we collected all the cells and incubated them with the PE Annexin V Apoptosis Detection Kit reagents (BD Pharmingen, Franklin Lake, New Jersey, USA) for 2 days. After 15 minutes of incubation, we observed the cells using CELL Quest software (BD Biosciences, San Jose, CA, USA). The proportion of apoptosis is reflected by the corresponding quadrant on the apoptosis map.

### **5-Ethynyl-2'-deoxyuridine (EdU) assay**

We inoculated the transfected cells in a 96-well plate at 10,000 per well and cultured them for 24 hours. The next day, we added EdU solution (RiboBio, China) to each well of the 96-well plate for incubation. After that, the cells were fixed and then were subjected to Apollo staining and DNA staining using Apollo reaction solution and Hoechst 33342, respectively. Finally, we observed the red and blue signals under the microscope to evaluate cell proliferation.

### **Fluorescent in situ hybridization (FISH)**

Cells were first fixed with 4% paraformaldehyde for 10 minutes and incubated in 70% ethanol overnight at 4°C. Next, the cells were permeabilized with 0.5% Triton X-100 for 5 minutes and washed with saline sodium citrate (SSC) buffer. Next, the cells were hybridized with a labelled FISH probe of circRNA at 37°C in hybridization buffer overnight. The cells were then washed with 4× sodium citrate buffer containing 0.1% Tween-20 for 5 minutes and washed with 1× SSC for 5 minutes. Finally, the cells were stained with 4,6-diamidino-2-phenylindole (DAPI) for 10 minutes. Images were captured using a fluorescence microscope.

### **Pull-down assay**

A biotin-labelled probe for circST3GAL6 was designed by RiboBio (Guangzhou, China). GC cells were harvested, lysed and incubated with the circST3GAL6 probe and oligo probe at 4°C overnight. The RNA mixture was bound to the magnetic beads with washing buffer several times. After that, the RNA was extracted using the RNeasy Mini Kit (QIAGEN, Germany) and detected by qRT-PCR. Biotinylated miR-300 and biotinylated miR-NC were produced by GenePharma (Shanghai, China), and the methods were the same as those described above.

### **Immunohistochemical (IHC) analysis of tissue samples**

The GC tissues were fixed with 10% formalin and embedded in paraffin. Next, the tissues were cut into sections and incubated with specific primary antibody at 4°C overnight. After washing twice, the sections were incubated with HRP-polymer-conjugated secondary antibody (abcam, UK) at 37°C for one hour. These sections were then stained with 3,3-diaminobenzidine solution and haematoxylin. Finally, we observed the slices via microscope. IHC score= Frequency\*intensity. The frequency was graded by the percentage of positive cells, which was grade 0, <5%; grade 1, 5~25%; grade 2, 25~50%; grade 3, 50~75%; grade 4, more than 75%. The intensity of cell staining was graded as 0 (negative), 1 (weak), 2 (moderate), and 3 (strong).

### **Transmission electron microscopy (TEM)**

We placed the cell pellet in a droplet of 2.5% glutaraldehyde in PBS buffer at pH 7.2 and fixed the cells overnight at 4 °C. The samples were then rinsed in PBS solution for 10 min three times and postfixed in 1% osmium tetroxide for 60 min at room temperature. Next, the samples were embedded in 10% gelatin, fixed in glutaraldehyde at 4 °C and cut into several blocks. Subsequently, the samples were dehydrated for 10 min in increasing concentrations of alcohol (30%, 50%, 70%, 90%, 95%, and 100% ×3). Next, we exchanged alcohol with propylene oxide and infiltrated samples with increasing concentrations (25%, 50%, 75%, and 100%) of Quetol-812 epoxy resin mixed with propylene oxide. Each step lasts at least 3 h. The samples were then embedded in pure Quetol-812 epoxy resin and polymerized at 35 °C for 12 h, 45 °C for 12 h, and 60 °C for 24 h. We cut samples into sections (100 nm) using an ultramicrotome and poststained them with uranyl acetate for 10 min and lead citrate for 5 min at room temperature. After that, we observed sections under a transmission electron microscope operated at 120 kV.

### **Nude mouse xenograft model**

In total,  $1 \times 10^6$  stably transfected GC cells or control cells were suspended in 100  $\mu$ l of PBS and injected into each armpit of 4-week-old female BALB/c nude mice purchased from the Department of Laboratory Animal Center of Nanjing Medical University. After 4 weeks, the mice were sacrificed, and the tumours were separated to measure their weights and volume. The tumour volume was calculated as  $V = \text{length} \times \text{width}^2 \times 0.5$ .

### **In vivo metastasis assay**

Stably transfected GC cells ( $1 \times 10^6$ ) were injected into the tail veins of 4-week-old female BALB/c nude mice. After 28 days, the bioluminescent signals of lung metastasis were detected using an IVIS Imaging system (Caliper Life Sciences, Hopkinton, MA, USA). After the mice were sacrificed, the lung metastatic lesions were assessed using haematoxylin and eosin (HE)-stained sections.

### **Luciferase reporter assay**

BGC-823 and SGC-7901 cells were seeded in 24-well plates and cotransfected with the corresponding plasmids and miRNA mimics. Luciferase reporter assays were conducted using a dual-luciferase reporter assay system (Promega, Madison, WI) according to the manufacturer's instructions after transfection for 48 hours. The relative luciferase activity was normalized to Renilla luciferase activity.

### **Confocal microscopy**

BGC-823 and SGC-7901 cells transfected with GFP-mRFP-LC3 lentivirus (GeneChem, China) were seeded into a 35-mm culture dish for confocal microscopy. The nucleus were stained with DAPI. Red and yellow puncta representing autolysosomes and autophagosomes, respectively, were detected by confocal microscopy (Carl Zeiss, Germany). Three random fields were selected for puncta quantification.

### **Chromatin immunoprecipitation assay**

ChIP assays were performed using the Magna ChIP™ A/G Chromatin Immunoprecipitation Kit (17-10085; Millipore Sigma, Burlington, Massachusetts, USA) according to the manufacturer's protocol. Briefly, cells were fixed with 37% formaldehyde and collected in lysis buffer. Chromatin fragments were sonicated on ice, and

then the lysates were immunoprecipitated with normal rabbit IgG and FOXP2 antibodies (5337; Cell Signaling Technology). Elution of the protein/DNA complexes was obtained after DNA purification using wash buffers and standard PCR. DNA was extracted for PCR amplification of specific DNA fragments.

## Statistics

The data were presented as means  $\pm$  SD in each experiment. A significant difference was considered at  $P < 0.05$  in each experiment. One-way analysis of variance (ANOVA) and Student's t-test were applied.

## Results

### CircST3GAL6 expression profiles in gastric cancer tissues and paired normal gastric tissues

To screen circRNAs involved in the progression of gastric cancer, circRNA-seq was used to analyse the expression of circRNAs in three pairs of gastric cancer tissues and adjacent normal tissues. Among 121 differentially expressed circRNAs, 76 were upregulated and 45 were downregulated ( $\text{FoldChange} \geq 2$  or  $\leq 0.5$ ,  $P < 0.05$ ). Next, we excluded circRNAs that were not included in circbase<sup>22</sup> and obtained 90 circRNAs. We chose the top 20 circRNAs to generate a heat map according to the fold change (Figure 1A). Circ\_0066608, which is also called circST3GAL6, attracted our attention because of its significantly low expression in gastric cancer (Figure 1B). To further verify the expression level of circST3GAL6 in gastric cancer tissues, we collected a cohort of 60 GC tissues and paired normal tissues, significantly downregulated expression of circST3GAL6 was detected via qRT-PCR (Figure 1C). Furthermore, we detected lower levels of circST3GAL6 in the HGC-27, MKN-45, MGC-803, BGC-823, and SGC-7901 GC cell lines than in the GES-1 cell line. BGC-823 cells showed the lowest expression of circST3GAL6, and SGC-7901 cells showed the second lowest expression of circST3GAL6 (Figure 1D). Therefore, we chose BGC-823 cells and SGC-7901 GC cells to investigate the downstream mechanism of circST3GAL6. Additionally, among the aforementioned patients, the expression level of circST3GAL6 was significantly correlated with GC tumour stage and tumour size (Table 1). Taken together, circST3GAL6 was significantly downregulated in GC tissues and GC cells, which deserved further study.

### Identification of the structure and characteristics of circST3GAL6

CircST3GAL6 is located at chromosome 3 and connected to head-to-tail splicing by exons 2-5, as confirmed by Sanger sequencing (Figure 1E). Next, we performed qRT-PCR with specially designed primers and discovered that circST3GAL6 resisted digestion by RNase R, but not linear ST3GAL6 or GAPDH (Figure 1F). Furthermore, we found that circST3GAL6 was more stable than linear ST3GAL6 in GC cells under actinomycin D treatment (Figure 1G). Additionally, PCR and agarose gel electrophoresis assays were performed to detect the expression level of ST3GAL6 in the cDNA and gDNA of GC cells compared with GAPDH. We detected circST3GAL6 in cDNA with different primers and found that circST3GAL6 could not be amplified by divergent primers, confirming that circST3GAL6 was not attributable to genomic rearrangements or PCR artefacts (Figure 1H). Fluorescence in situ hybridization (FISH) analysis and qRT-PCR analysis of nuclear and cytoplasmic RNA demonstrated that circST3GAL6 was located mostly in the

cytoplasm of GC cells (Figure 1I, Figure 1J). Thus, these results indicated that circST3GAL6 is a stable circRNA located in the cytoplasm.

### **CircST3GAL6 inhibits proliferation and metastasis and promotes apoptosis and autophagy of GC cells in vitro.**

To determine whether circST3GAL6 affects the biological behaviour of GC cells, we designed specific small interfering RNAs (siRNAs) to silence the expression of circST3GAL6 and constructed a circST3GAL6 overexpression plasmid, which was transfected into BGC-823 and SGC-7901 cells. The transfection efficiency of circST3GAL6 was verified by qRT-PCR, while ST3GAL6 mRNA was not affected (Figure 2A). Next, we performed CCK-8, EdU, colony formation, and Transwell assays to verify the proliferation and invasion of circST3GAL6. We observed that circST3GAL6 overexpression significantly inhibited the cell proliferation rate (Figure 2B-D, Figure S1A-C) and promoted cell apoptosis (Figure 2F), as indicated by CCK-8, colony formation, EdU, and Annexin V-FITC apoptosis detection assays in BGC-823 and SGC-7901 cells. Additionally, knockdown of circST3GAL6 obviously promoted cell proliferation and inhibited cell apoptosis compared with the negative control in BGC-823 and SGC-7901 cells (Figure 2B-D, Figure S1A-C). These results showed that circST3GAL6 was connected with GC cell growth. To verify the relationship of circST3GAL6 and cell apoptosis, the relevant apoptosis proteins were detected by western blotting. As shown in Figure 2H and Figure S1F, circST3GAL6 overexpression significantly increased the level of cleaved caspase-3, while the expression level of Bcl2 was downregulated and circST3GAL6 knocking down showed the opposite results. Since apoptosis has been reported to affect the level of autophagy<sup>23,24</sup>, we tried to discover whether circST3GAL6 affects autophagy. GFP/mRFP-LC3 dot accumulation was observed by overexpressing circST3GAL6, while circST3GAL6 knockdown showed opposite results (Figure 2G, S1E). Next, we detected p62 and LC3 I/II levels in GC cells by western blotting, and circST3GAL6 overexpression increased the ratio of LC3 II/I and reduced p62 expression in BGC-823 and SGC-7901 cells (Figure 2H, S1F). Additionally, we found that circST3GAL6 overexpression reduced the migration and invasion of GC cells, while circST3GAL6 knockdown showed opposite results (Figure 2E, S1D) via using the Transwell assay, indicating that circST3GAL6 was relevant to GC cell metastasis. Because the epithelial to mesenchymal transition (EMT) is closely correlated with GC cell migration and invasion<sup>25</sup>, we investigated the role of circST3GAL6 in regulating EMT-related factors. We observed reduced expression of vimentin, snail, slug and N-cadherin and upregulated E-cadherin expression in BGC-823 and SGC-7901 cells transfected with the circST3GAL6 overexpression plasmids. Meanwhile, GC cells transfected with siRNA displayed the opposite results. (Figure 2H, S1F). Collectively, these results suggest that circST3GAL6 is a key factor that inhibits the proliferation, migration, and invasion of GC cells.

### **CircST3GAL6 inhibits tumour growth and metastasis in vivo**

To investigate the potential role of circST3GAL6 in vivo, we subcutaneously injected  $1 \times 10^6$  GC cells into nude mice transfected with circST3GAL6 overexpression or sh-circST3GAL6. After four weeks, all the mice in the

three groups were sacrificed, and tumours were measured and weighed separately (Figure 3A). Significant decreases in the tumour weight and volume were observed in the circST3GAL6 overexpression group for both cell lines compared with those in the negative control group, while sh-circST3GAL6 showed opposite results (Figure 3B). Next, immunohistochemical staining of Ki-67 was performed in the tumour tissues. Lower expression of Ki-67 in tumour tissues was observed in the circST3GAL6 overexpression group while the tumour tissues with knock down of circST3GAL6 showed the stronger Ki-67 staining (Figure 3C). Furthermore, a lung metastasis model was generated to detect the ability of circST3GAL6 to inhibit tumour metastasis. After injecting cells into the tail veins of nude mice for four weeks, luciferase signals were detected. CircST3GAL6 overexpression significantly inhibited metastasis to the lung, while circST3GAL6 knockdown promoted lung metastasis (Figure 3D). The lung tissues of mice were separated, and haematoxylin-eosin staining was performed to confirm the formation of lung metastases, the results of which were consistent with the luciferase signal (Figure 3E). In conclusion, these results indicate that circST3GAL6 inhibits tumorigenesis and metastasis in vivo.

### **CircST3GAL6 functions as a sponge of miR-300**

Many articles have reported that circRNAs can work as miRNA sponges and regulate downstream genes in tumour development<sup>26, 27</sup>. We predicted the target miRNAs of circST3GAL6 using two prediction databases: miRanda<sup>28</sup> and PITA<sup>29</sup>. According to the intersection of these two databases, seven miRNAs (hsa-miR-300, hsa-miR-370-5p, hsa-miR-510-5p, hsa-miR-6758-5p, hsa-miR-6832-5p, hsa-miR-6859-5p, and hsa-miR-877-5p) were selected based on binding scores (Figure 4A). To absorb circST3GAL6-related miRNAs, we used a specific biotin-labelled circST3GAL6 via pull-down assays. The efficiency of the circST3GAL6 probe is shown in Figure 4B. We then used a qRT-PCR assay to analyse the expression levels of the seven miRNAs from the circST3GAL6 pull-down experiments in BGC-823 and SGC-7901 cells. Among these miRNAs, we only found the enrichment of miR-300 of circST3GAL6 in both BGC-823 and SGC-7901 cell lines, while the other miRNAs did not show such close interactions with circST3GAL6 (Figure 4C). Additionally, we predicted two binding sites between circST3GAL6 and miR-300, and the luciferase reporter assay was performed to confirm the direct binding between circST3GAL6 and miR-300 via their complementary sequence (Figure 4D). When we cotransfected wild-circST3GAL6 and miR-300, we observed a significant reduction in luciferase reporter activity relative to cotransfection with control RNA in BGC-823 and SGC-7901 cells. Next, we mutated two binding sites in the circST3GAL6 sequence and found that the cotransfection of miR-300 and mut-circST3GAL6, with both binding sites mutated, did not significantly reduce the luciferase signal (Figure 4E). In conclusion, the direct interaction between circST3GAL6 and miR-300 was confirmed. Moreover, we performed FISH assays in BGC-823 and SGC-7901 cells and found that miR-300 was located in the cytoplasm with circST3GAL6 (Figure 4F). A significantly upregulated expression of miR-300 was detected via qRT-PCR on 60 paired GC tissues and adjacent normal tissues (Figure 4G). Meanwhile, we proved a clear negative correlation between the expression level of circST3GAL6 and miR-300 (Figure 4H). According to the clinical data of the aforementioned patients, the expression level of miR-300 was significantly correlated with GC tumour size (Table 1). Collectively, these results indicated that circST3GAL6 functions as a sponge of miR-300.

## Overexpression of miR-300 reverses the effect of circST3GAL6 on GC cells

To determine whether circST3GAL6 promoted malignant biological functions in GC cell lines via the circST3GAL6/miR-300 axis, we performed rescue experiments. First, we detected the transfection efficiency of miR-300 inhibitors and mimics (Figure 5A). Overexpression of miR-300 promoted the proliferation and migration of GC cells and inhibited GC cell apoptosis, as determined by EdU, colony formation, Transwell migration assays and Annexin V-FITC apoptosis detection assays (Figure 5B-E, Figure S2A-C). Furthermore, the negative effect of circST3GAL6 overexpression on proliferation and invasion and the promotion of apoptosis was restored by miR-300 mimics (Figure 5B-E, Figure S2A-C). Apoptosis- and EMT-related protein expression was subsequently detected using western blotting. The effect of circST3GAL6 overexpression on cleaved caspase-3, bcl-2 and EMT-related protein levels was restored by miR-300 mimics (Figure 5G, Figure S2E). Since circST3GAL6 has been confirmed to be related to autophagy in the above study, we further explored the effect of miR-300 on autophagy. Interestingly, we found that miR-300 mimics reversed the increase in GFP/mRFP-LC3 dots caused by transfection of the circST3GAL6 overexpression plasmid into BGC-823 and SGC-7901 GC cells (Figure 5F, Figure S2D). Increased ratio of LC3 II/I and reduced p62 protein level caused by circST3GAL6 overexpression were reversed by miR-300 mimics. (Figure 5G, Figure S2E). These results indicated that circST3GAL6 could play a tumour-suppressive role and regulate autophagy by sponging miR-300.

## FOXP2 is a target of circST3GAL6 by sponging miR-300

Based on the results above, we further investigated the downstream mechanism of miR-300. We employed miRWalk<sup>30</sup>, miRDB<sup>31</sup> and TargetScan<sup>32</sup> and combined with the significantly downregulated genes in TCGA GC database. Ten genes overlapped (Figure 6A) and qRT-PCR indicated that the mRNA level of FOXP2 was significantly upregulated in both BGC823 and SGC-7901 cells transfected with the miR-300 inhibitors compared with those transfected with the negative control, illustrating that FOXP2 may be a direct target of miR-300 in GC (Figure 6B). The bioinformatics database TargetScan was used to predicted the potential binding site with miR-300 in the 3'UTR of FOXP2 (Figure 6C). Dual-luciferase reporter assays were performed to verify whether miR-300 could target FOXP2 directly. As shown in Figure 6D, we found that miR-300 overexpression significantly decreased the luciferase activity of wild-type FOXP2 but not mutant FOXP2 in GC cells, indicating that miR-300 could bind to the FOXP2 3'UTR. TCGA database showed that FOXP2 was significantly downregulated in gastric cancer tissues (Figure 6E). Additionally, qRT-PCR revealed that FOXP2 expression was lower in 60 paired GC tumour tissues than in normal tissues (Figure 6F). The positive correlation between the expression level of circST3GAL6 and FOXP2 was also proved (Figure 6G). Subsequently, western blotting and qRT-PCR were used to observe FOXP2 expression in human GC cells. CircST3GAL6 overexpression increased the expression level of FOXP2, which could be restored by miR-300 mimics (Figure 6H, Figure S3A). Finally, we confirmed lower levels of FOXP2 in GC tissues than in adjacent normal tissues by performing immunohistochemistry analysis of 12 paired GC tumour tissues and paired normal stomach tissues (Figure 6I). On the basis of the above results, we proved the potential regulation of FOXP2 by circST3GAL6 through sponging miR-300.

## **Knockdown of FOXP2 reverses the effect of miR-300 inhibitors on GC cells**

Because we have proved that circST3GAL6 plays a tumour-suppressive role by sponging miR-300 and FOXP2 is the target gene of miR-300, we investigated how circST3GAL6 regulates FOXP2 via miR-300 and its effects on GC cells. The transfection efficiency of FOXP2 siRNAs and overexpression plasmids was verified (Figure 7A). The promotion of proliferation and migration of GC cells caused by miR-300 knockdown could be restored via FOXP2 knockdown (Figure 7B-D, Figure S3B-D). Transfection with miR-300 inhibitors promoted GC cell apoptosis, and FOXP2 knockdown restored this effect (Figure 7E). The levels of cleaved caspase-3, bcl-2 and EMT-related proteins were further detected by western blotting (Figure 7G, Figure S3F). Furthermore, we found that FOXP2 knockdown reversed the increase in GFP/mRFP-LC3 dots caused by transfection with miR-300 inhibitors in BGC-823 and SGC-7901 GC cells (Figure 7F, Figure S3E). Additionally, knockdown of miR-300 increased the ratio of LC3 II/I and reduced P62 expression, which could be recovered by cotransfection with FOXP2 siRNAs (Figure 7G, Figure S3F). Combined with the above results, we proved that circST3GAL6 markedly regulates FOXP2 expression and regulate autophagy by sponging miR-300.

## **FOXP2 transcriptionally inhibits MET and regulates autophagy**

We proved that circST3GAL6 promoted autophagy via the miR-300/FOXP2 axis, but the downstream mechanism of FOXP2 remains to be explored. It was reported that FOXP2 is a transcription factor that binds to the Met promoter and suppresses its expression<sup>19</sup> and the negative correlation between FOXP2 and Met was confirmed from the TCGA database (Figure S4A). As a receptor tyrosine kinase, Met transduces signals from the extracellular matrix into the cytoplasm by binding to hepatocyte growth factor (HGF) ligand and regulates a variety of physiological processes, including proliferation, migration, morphogenesis, and survival. On the basis of above results, we tried to investigate whether FOXP2 regulated autophagy through Met. Next, we searched the possible binding sites with FOXP2 on the promoter of Met 0-2000 bp upstream using JASPAR (Figure 8A). Because most of the predicted sites were located between -1000 bp and +1 bp of the promoter sequence, two possible binding sites were confirmed according to the binding score (Figure 8A). We constructed three PGL3 luciferase reporter gene vectors of FOXP2 promoter regions that covered the potential binding sites (Figure 8A). FOXP2 overexpression significantly increased the luciferase activity of P1 but not P3, indicating that FOXP2 could bind to the -1000 region on the Met promoter (Figure 8B). Furthermore, we used the chromatin immunoprecipitation (ChIP) assay to detect binding sites between FOXP2 and the Met promoter region. The pulled-down DNA region was amplified by qRT-PCR, and the negative control could not bind to FOXP2. qRT-PCR illustrated that amplification of the pulled-down DNA region using Primer 2 was significantly higher than that using Primer 3 (Figure 8C-D, S4B). These results showed that FOXP2 directly bound to binding site A on the promoter of Met. Met activates downstream signalling pathways, including the PI3K-Akt-mTOR pathway, which is a classical pathway that regulates autophagy<sup>33, 34</sup>. Western blot assays were applied to detect the downstream signalling pathways of FOXP2. Knockdown of FOXP2 significantly increased the expression of Met, phospho-AKT (T308,

S473) and phospho-mTOR (S2448) and these effects were reversed by Met silencing (Figure 8E, S4D). Knock down of FOXP2 reduced the ratio of LC3 II/I and increased P62 expression, which could be restored by downregulated Met (Figure 8E, S4D). These results were also confirmed by GFP/mRFP-LC3 dot analysis and TEM (Figure 8F, S4C). Furthermore, we investigated whether GC cell proliferation and migration affected by circST3GAL6 through FOXP2 were regulated by autophagy. 3-MA (3-Methyladenine, an autophagy inhibitor) was used to study whether the above statement was true. FOXP2 overexpression promoted autophagy, which could be suppressed by 3-MA through GFP/mRFP-LC3 dots, TEM and western blotting (Figure 8H-J, Figure S5A-B). Subsequently, inhibition of cell proliferation and invasion induced by FOXP2 overexpression was restored by 3-MA (Figure 8K-N, S5C-F). Thus, we demonstrated that circST3GAL6 regulates the AKT/mTOR pathway through FOXP2 transcriptional inhibition of Met to affect autophagy, thereby regulating the proliferation and invasion of gastric cancer cells (Figure 8O).

## Discussion

Gastric cancer (GC) ranks fifth in incidence of all cancers worldwide, and its incidence is particularly high in East Asia, including China<sup>1,2</sup>. New targets are warranted for GC treatment. In our study, next-generation sequencing was performed to detect the differential expression of circRNAs in GC tissues compared with that in adjacent normal stomach tissues. After screening the sequencing results, circST3GAL6 was selected because of its high fold-change and significant P value, which may play an important role in GC. This is the first report showing the circular RNA ST3GAL6 can inhibit the malignant progression of gastric cancer. According to previous studies, linear ST3GAL6 is involved in the progression of multiple tumours, including urinary bladder cancer, colorectal cancer and multiple myeloma<sup>35-37</sup>, suggesting a potential connection between the two forms. Furthermore, we confirmed the lower expression of circST3GAL6 in GC tissues and its correlation with tumour size and stage, which was expected to be one of the biomarkers for detecting gastric cancer.

CircRNAs affect cancer progression by acting as miRNA sponges and RNA-binding proteins (RBPs)<sup>38</sup>; they can even be translated into proteins<sup>39</sup>. Our results proved that circST3GAL6 could serve as a sponge of miR-300, forming a natural competitive endogenous RNA network. Our results confirmed that only miR-300 could be pulled down via the circST3GAL6 probe in both GC cell lines. Several reports demonstrated that circRNAs could impact RBPs and that some RBPs could even affect the expression of circRNAs in turn<sup>40</sup>. We tried to predict whether some RBPs could bind to circST3GAL6 via RBPmap (<http://rbpmap.technion.ac.il/>), and the results showed that KHDRBS1 might have a connection with circST3GAL6. Although KHDRBS1 promoted pre-mRNA circularization, we found that KHDRBS1 could not affect the expression of circST3GAL6 when it was knocked down. There may be some downstream RBPs still to be discovered.

The forkhead box P (FOXP) family is considered a transcription factor<sup>15</sup>, and FOXP2 was predicted and confirmed to be the target gene of miR-300. Because FOXP2 played a vital role in regulating gene transcription, we predicted the potential binding sites of the promoter of MET via JASPAR<sup>19</sup>. The transcription of MET via FOXP2 was verified by the luciferase assay and CHIP assay. MET is a member of the receptor tyrosine kinase family. The Met receptor binds to its ligand, hepatocyte growth factor (HGF), to induce the

dimerization of Met, causing it to enter an active state, where it phosphorylates its substrate and activates downstream signalling pathways, including the PI3K-Akt-mTOR and MAPK/ERK pathways<sup>41, 42</sup>. Since circST3GAL6 regulated autophagy in our previous experiments and circST3GAL6 could affect MET by binding FOXP2 via miR-300, we further verified whether circST3GAL6 affected autophagy via the FOXP2/MET axis. CircST3GAL6 further regulated autophagy by affecting mTOR phosphorylation through FOXP2-mediated MET transcriptional inhibition. Furthermore, we found that GC cell proliferation and migration were altered after applying the autophagy inhibitor 3-MA. Although autophagy was reported to regulate cell proliferation, migration and apoptosis<sup>43-46</sup>, the specific mechanism remains to be explored and confirmed in vivo.

## Conclusion

We confirmed that circST3GAL6 was significantly downregulated in GC cells and tissues. CircST3GAL6 overexpression inhibits the malignant progression of gastric cancer through autophagy regulated by the FOXP2/MET/mTOR axis. These findings indicate that circST3GAL6 may be a potential therapeutic target for GC.

## Declarations

### Authors' contributions

XZ and JC participated in the experimental design and data analysis. JY performed some of the experiments and were responsible for quality control. PX performed the experiments and wrote the manuscript. All of the authors read and approved the final manuscript.

### Ethics approval and consent to participate

This research was approved by the Ethics Committee of the First Affiliated Hospital of Nanjing Medical University. The experiments concerning animals were approved by the Nanjing Medical University Ethics Committee.

### Competing interests

The authors declare that they have no competing interests.

## Abbreviations

GC: Gastric cancer; ceRNA: Competitive endogenous RNA; circRNA: Circular RNA; miRNA: MicroRNA; RBP: RNA-binding protein; qRT-PCR: Quantitative real-time polymerase chain reaction; FISH: RNA fluorescence in situ hybridization; EdU: 5-Ethynyl-2'-deoxyuridine; IHC: Immunohistochemistry; HE: Hematoxylin-eosin; RIP: RNA immunoprecipitation; gDNA: Genomic DNA; EMT: Epithelial-mesenchymal transition; 3'-UTR:

3'Untranslated region; TEM: Transmission electron microscopy; FOXP2: Forkhead box p2; 3-MA: 3-Methyladenine

## References

1. Bray F, Ferlay J, Soerjomataram I, Siegel RL, Torre LA, Jemal A. Global cancer statistics 2018: GLOBOCAN estimates of incidence and mortality worldwide for 36 cancers in 185 countries. *CA Cancer J Clin.* Nov 2018;68(6):394-424. doi:10.3322/caac.21492
2. Chen W, Zheng R, Baade PD, et al. Cancer statistics in China, 2015. *CA Cancer J Clin.* Mar-Apr 2016;66(2):115-32. doi:10.3322/caac.21338
3. Sah B, Zhang B, Zhang H, et al. Neoadjuvant FLOT versus SOX phase II randomized clinical trial for patients with locally advanced gastric cancer. *Nature communications.* 2020;11(1):6093. doi:10.1038/s41467-020-19965-6
4. Shitara K, Van Cutsem E, Bang Y, et al. Efficacy and Safety of Pembrolizumab or Pembrolizumab Plus Chemotherapy vs Chemotherapy Alone for Patients With First-line, Advanced Gastric Cancer: The KEYNOTE-062 Phase 3 Randomized Clinical Trial. *JAMA oncology.* 2020;6(10):1571-1580. doi:10.1001/jamaoncol.2020.3370
5. Liu F, Huang C, Xu Z, et al. Morbidity and Mortality of Laparoscopic vs Open Total Gastrectomy for Clinical Stage I Gastric Cancer: The CLASS02 Multicenter Randomized Clinical Trial. *JAMA oncology.* 2020;6(10):1590-1597. doi:10.1001/jamaoncol.2020.3152
6. Allemani C, Weir H, Carreira H, et al. Global surveillance of cancer survival 1995-2009: analysis of individual data for 25,676,887 patients from 279 population-based registries in 67 countries (CONCORD-2). *Lancet (London, England).* 2015;385(9972):977-1010. doi:10.1016/s0140-6736(14)62038-9
7. Goodall G, Wickramasinghe V. RNA in cancer. *Nature reviews Cancer.* 2021;21(1):22-36. doi:10.1038/s41568-020-00306-0
8. Saaoud F, Drummer I V C, Shao Y, et al. Circular RNAs are a novel type of non-coding RNAs in ROS regulation, cardiovascular metabolic inflammations and cancers. *Pharmacology & therapeutics.* 2020:107715. doi:10.1016/j.pharmthera.2020.107715
9. Wen G, Zhou T, Gu W. The potential of using blood circular RNA as liquid biopsy biomarker for human diseases. *Protein & cell.* 2020;doi:10.1007/s13238-020-00799-3
10. Gao W, Guo H, Niu M, et al. circPARD3 drives malignant progression and chemoresistance of laryngeal squamous cell carcinoma by inhibiting autophagy through the PRKCI-Akt-mTOR pathway. *Molecular cancer.* 2020;19(1):166. doi:10.1186/s12943-020-01279-2
11. Okholm T, Sathe S, Park S, et al. Transcriptome-wide profiles of circular RNA and RNA-binding protein interactions reveal effects on circular RNA biogenesis and cancer pathway expression. *Genome medicine.*

2020;12(1):112. doi:10.1186/s13073-020-00812-8

12. Wu X, Xiao S, Zhang M, et al. A novel protein encoded by circular SMO RNA is essential for Hedgehog signaling activation and glioblastoma tumorigenicity. *Genome biology*. 2021;22(1):33. doi:10.1186/s13059-020-02250-6
13. Ma C, Wang X, Yang F, et al. Circular RNA hsa\_circ\_0004872 inhibits gastric cancer progression via the miR-224/Smad4/ADAR1 successive regulatory circuit. *Molecular cancer*. 2020;19(1):157. doi:10.1186/s12943-020-01268-5
14. Chen L, Wang L, Ren Y, et al. The circular RNA circ-ERBIN promotes growth and metastasis of colorectal cancer by miR-125a-5p and miR-138-5p/4EBP-1 mediated cap-independent HIF-1 $\alpha$  translation. *Molecular cancer*. 2020;19(1):164. doi:10.1186/s12943-020-01272-9
15. Kim J, Hwang J, Jung J, Lee H, Lee D, Kim S. Molecular networks of FOXP family: dual biologic functions, interplay with other molecules and clinical implications in cancer progression. *Molecular cancer*. 2019;18(1):180. doi:10.1186/s12943-019-1110-3
16. Chandra A, Goldman N, Vahedi G. Foxp3 Re-distributes Its Heavy Lifting. *Immunity*. 2020;53(5):895-897. doi:10.1016/j.immuni.2020.10.021
17. van der Veecken J, Glasner A, Zhong Y, et al. The Transcription Factor Foxp3 Shapes Regulatory T Cell Identity by Tuning the Activity of trans-Acting Intermediaries. *Immunity*. 2020;53(5):971-984.e5. doi:10.1016/j.immuni.2020.10.010
18. Li H, Xue Y, Ma J, et al. SNHG1 promotes malignant biological behaviors of glioma cells via microRNA-154-5p/miR-376b-3p- FOXP2- KDM5B participating positive feedback loop. *J Exp Clin Cancer Res*. Feb 6 2019;38(1):59. doi:10.1186/s13046-019-1063-9
19. Mukamel Z, Konopka G, Wexler E, et al. Regulation of MET by FOXP2, genes implicated in higher cognitive dysfunction and autism risk. *J Neurosci*. Aug 10 2011;31(32):11437-42. doi:10.1523/JNEUROSCI.0181-11.2011
20. Gan X, Zhu H, Jiang X, et al. CircMUC16 promotes autophagy of epithelial ovarian cancer via interaction with ATG13 and miR-199a. *Mol Cancer*. Feb 28 2020;19(1):45. doi:10.1186/s12943-020-01163-z
21. Lin X, Peng Z, Wang X, et al. Targeting autophagy potentiates antitumor activity of Met-TKIs against Met-amplified gastric cancer. *Cell Death Dis*. Feb 13 2019;10(2):139. doi:10.1038/s41419-019-1314-x
22. Glazar P, Papavasileiou P, Rajewsky N. circBase: a database for circular RNAs. *RNA*. Nov 2014;20(11):1666-70. doi:10.1261/rna.043687.113
23. Marino G, Niso-Santano M, Baehrecke EH, Kroemer G. Self-consumption: the interplay of autophagy and apoptosis. *Nat Rev Mol Cell Biol*. Feb 2014;15(2):81-94. doi:10.1038/nrm3735

24. Chen Q, Kang J, Fu C. The independence of and associations among apoptosis, autophagy, and necrosis. *Signal Transduct Target Ther.* 2018;3:18. doi:10.1038/s41392-018-0018-5
25. Mittal V. Epithelial Mesenchymal Transition in Tumor Metastasis. *Annual Review of Pathology: Mechanisms of Disease.* 2018;13(1):395-412. doi:10.1146/annurev-pathol-020117-043854
26. Fan Y, Wang J, Jin W, et al. CircNR3C2 promotes HRD1-mediated tumor-suppressive effect via sponging miR-513a-3p in triple-negative breast cancer. *Molecular cancer.* 2021;20(1):25. doi:10.1186/s12943-021-01321-x
27. Li Y, Zhang Y, Zhang S, et al. circRNA circARNT2 Suppressed the Sensitivity of Hepatocellular Carcinoma Cells to Cisplatin by Targeting the miR-155-5p/PDK1 Axis. *Molecular therapy Nucleic acids.* 2021;23:244-254. doi:10.1016/j.omtn.2020.08.037
28. John B, Enright AJ, Aravin A, Tuschl T, Sander C, Marks DS. Human MicroRNA targets. *PLoS Biol.* Nov 2004;2(11):e363. doi:10.1371/journal.pbio.0020363
29. Kertesz M, Iovino N, Unnerstall U, Gaul U, Segal E. The role of site accessibility in microRNA target recognition. *Nat Genet.* Oct 2007;39(10):1278-84. doi:10.1038/ng2135
30. Sticht C, De La Torre C, Parveen A, Gretz N. miRWalk: An online resource for prediction of microRNA binding sites. *PLoS One.* 2018;13(10):e0206239. doi:10.1371/journal.pone.0206239
31. Wong N, Wang X. miRDB: an online resource for microRNA target prediction and functional annotations. *Nucleic Acids Res.* Jan 2015;43(Database issue):D146-52. doi:10.1093/nar/gku1104
32. Agarwal V, Bell GW, Nam JW, Bartel DP. Predicting effective microRNA target sites in mammalian mRNAs. *Elife.* Aug 12 2015;4doi:10.7554/eLife.05005
33. Eslami M, Yousefi B, Kokhaei P, Arabkari V, Ghasemian A. Current information on the association of Helicobacter pylori with autophagy and gastric cancer. *Journal of cellular physiology.* 2019;doi:10.1002/jcp.28279
34. Cai H, Yu Y, Ni X, et al. LncRNA LINC00998 inhibits the malignant glioma phenotype via the CBX3-mediated c-Met/Akt/mTOR axis. *Cell death & disease.* 2020;11(12):1032. doi:10.1038/s41419-020-03247-6
35. Jia Y, Zhou J, Tan T, et al. Myeloma-specific superenhancers affect genes of biological and clinical relevance in myeloma. *Blood cancer journal.* 2021;11(2):32. doi:10.1038/s41408-021-00421-7
36. Dalangood S, Zhu Z, Ma Z, et al. Identification of glycogene-type and validation of ST3GAL6 as a biomarker predicts clinical outcome and cancer cell invasion in urinary bladder cancer. *Theranostics.* 2020;10(22):10078-10091. doi:10.7150/thno.48711
37. Hu J, Shan Y, Ma J, et al. LncRNA ST3Gal6-AS1/ST3Gal6 axis mediates colorectal cancer progression by regulating  $\alpha$ -2,3 sialylation via PI3K/Akt signaling. *International journal of cancer.* 2019;145(2):450-460. doi:10.1002/ijc.32103

38. Liang Y, Wang H, Chen B, et al. circDCUN1D4 suppresses tumor metastasis and glycolysis in lung adenocarcinoma by stabilizing TXNIP expression. *Molecular therapy Nucleic acids*. 2021;23:355-368. doi:10.1016/j.omtn.2020.11.012
39. Ho-Xuan H, Glažar P, Latini C, et al. Comprehensive analysis of translation from overexpressed circular RNAs reveals pervasive translation from linear transcripts. *Nucleic acids research*. 2020;48(18):10368-10382. doi:10.1093/nar/gkaa704
40. Shi L, Yan P, Liang Y, et al. Circular RNA expression is suppressed by androgen receptor (AR)-regulated adenosine deaminase that acts on RNA (ADAR1) in human hepatocellular carcinoma. *Cell death & disease*. 2017;8(11):e3171. doi:10.1038/cddis.2017.556
41. Guo R, Luo J, Chang J, Rekhtman N, Arcila M, Drilon A. MET-dependent solid tumours - molecular diagnosis and targeted therapy. *Nature reviews Clinical oncology*. 2020;17(9):569-587. doi:10.1038/s41571-020-0377-z
42. Recondo G, Che J, Jänne P, Awad M. MET Targeting Dysregulation in Cancer. *Cancer discovery*. 2020;10(7):922-934. doi:10.1158/2159-8290.Cd-19-1446
43. Liang Y, Pi H, Liao L, et al. Cadmium promotes breast cancer cell proliferation, migration and invasion by inhibiting ACS2/ATG5-mediated autophagy. *Environmental pollution (Barking, Essex : 1987)*. 2021;273:116504. doi:10.1016/j.envpol.2021.116504
44. Li C, Li Y, Zhuang M, et al. Long noncoding RNA H19 act as a competing endogenous RNA of Let-7g to facilitate IEC-6 cell migration and proliferation via regulating EGF. *Journal of cellular physiology*. 2021;236(4):2881-2892. doi:10.1002/jcp.30061
45. Wu Q, Ma J, Wei J, Meng W, Wang Y, Shi M. lncRNA SNHG11 Promotes Gastric Cancer Progression by Activating the Wnt/ $\beta$ -Catenin Pathway and Oncogenic Autophagy. *Molecular therapy : the journal of the American Society of Gene Therapy*. 2020;doi:10.1016/j.ymthe.2020.10.011
46. Xu K, He Y, Moqbel S, Zhou X, Wu L, Bao J. SIRT3 ameliorates osteoarthritis via regulating chondrocyte autophagy and apoptosis through the PI3K/Akt/mTOR pathway. *International journal of biological macromolecules*. 2021;175:351-360. doi:10.1016/j.ijbiomac.2021.02.029

## Table

**Table 1** Expression of circST3GAL6 and miR-300 in human gastric cancer and the clinicopathological characteristics of the patients'

\*p < 0.05 and \*\*p < 0.01 Statistically significant difference

Parameters	Group	circSTGAL6 expression				miR-300 expression			
		Cases	Low	High	P-value	Cases	Low	High	P-value
Gender									
	female	18	10	8	0.5731	18	11	7	0.2598
	male	42	20	22		42	19	23	
Age at surgey									
	≥55	47	24	23	0.754	47	22	25	0.3472
	<55	13	6	7		13	8	5	
T grade									
	T1+T2	19	11	8	0.4051	19	9	10	0.4051
	T3+T4	31	19	22		31	11	20	
Lymphatic invasion									
	Negative(N0)	8	2	6	0.1287	8	3	5	0.4475
	Positive(N1-N3)	52	28	24		52	27	25	
Tumor site									
	Cardiac	24	10	14	0.2918	24	11	13	0.5982
	Non-cardiac	36	20	16		36	19	17	
Stage									
	I-II	22	7	15	0.0321 *	22	13	9	0.2839
	III-IV	38	23	15		38	17	21	
Size(cm)									
	<3	39	14	25	0.0029**	39	24	15	0.0149*
	≥3	21	16	5		21	6	15	
Lauren classification									
	intestinal type carcinoma	21	13	8	0.1760	21	9	12	0.4168
	diffuse gastric carcinoma	39	17	22		39	21	18	

p<0.05 represents statistical significance (Chi-square test)

## Figures



treated with RNase R to detect their stability via qRT-PCT. g. qRT-PCR analysis of circST3GAL6 and ST3GAL6 after actinomycin D treatment. h. qRT-PCR products of linear and circular products amplified with convergent and divergent primers in cDNA and genomic DNA (gDNA) compared to GAPDH. i. FISH experiments showed that CircST3GAL6 was mostly located in the cytoplasm. j. The proportion of circST3GAL6 in the nucleus and cytoplasm was confirmed by qRT-PCR. (\* $p < 0.05$ , \*\* $p < 0.01$ , \*\*\* $p < 0.001$ . Data are expressed as the means  $\pm$  SDs)

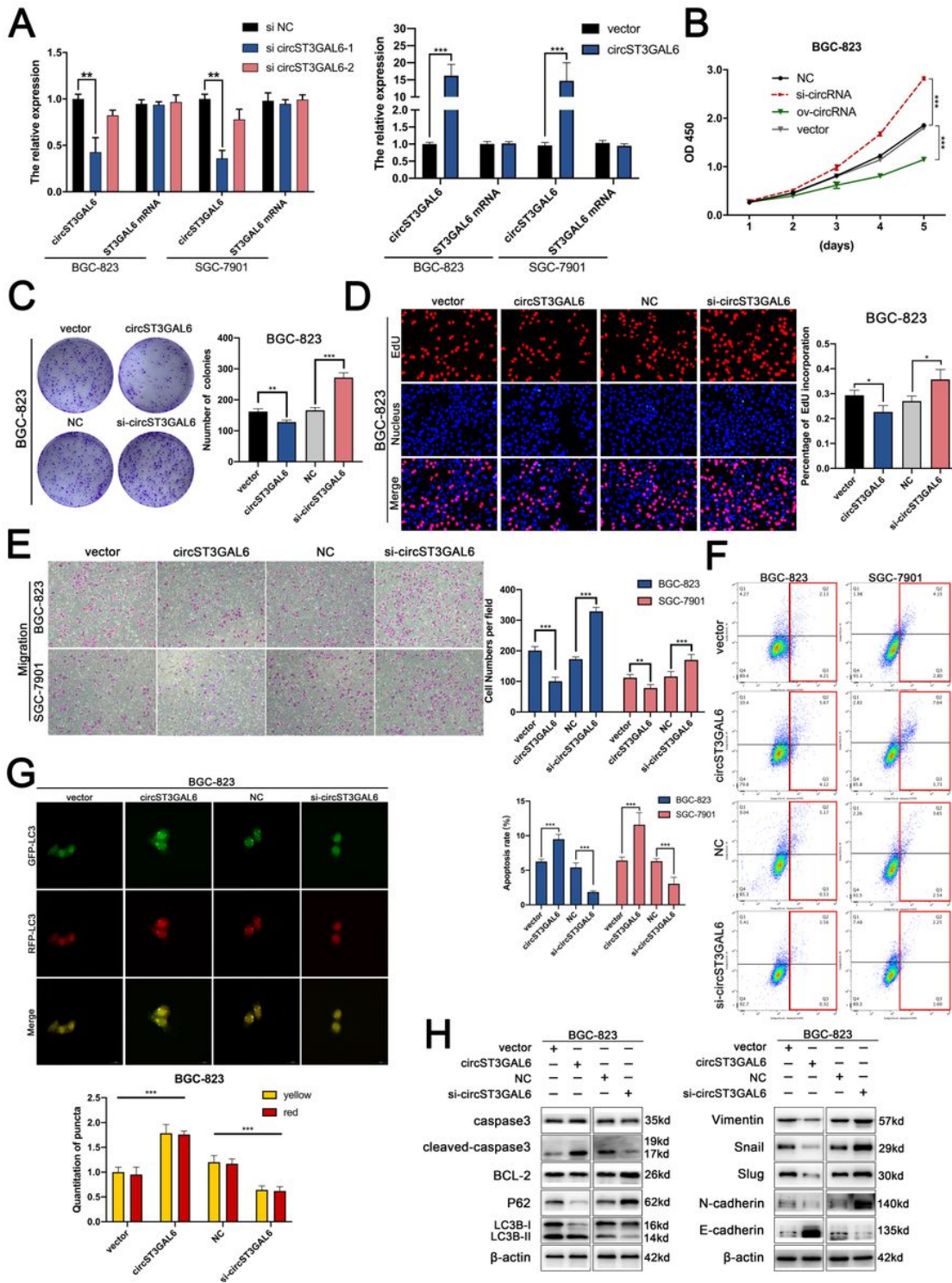
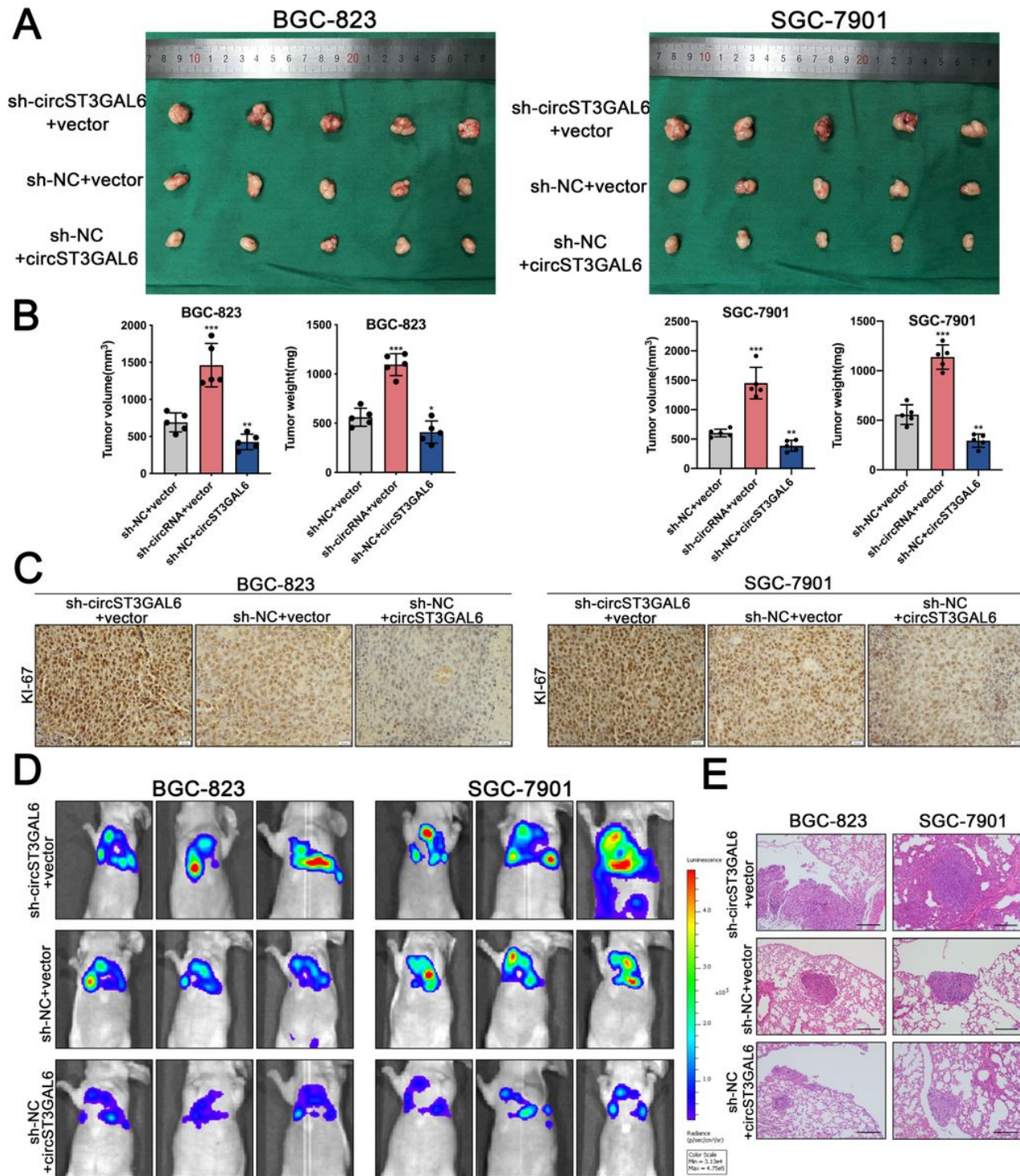


Figure 2

CircST3GAL6 inhibits the proliferation, metastasis and promotes apoptosis/autophagy of GC cells in vitro. a. qRT-PCR analysis of circST3GAL6 and ST3GAL6 mRNA expression after treatment with two siRNAs and an overexpression plasmid. b. The proliferation of BGC-823 cells transfected with circST3GAL6 siRNA or an overexpression plasmid by a CCK-8 assay. c-d. Assessment of BGC-823 cell proliferation by colony formation assay and EdU assay e. Assessment of cell migration by transwell assay in BGC-823 and SGC-7901 cells. f. Flow cytometric analysis of the apoptosis of BGC-823 and SGC-7901 cells. g. GFP/mRFP-LC3 dots in BGC-823 cell were observed and counted by confocal microscopy, scale bar = 20 $\mu$ m. h. Detection of apoptosis, autophagy and EMT related proteins by western blotting in BGC823 cells. (\*p < 0.05, \*\*p < 0.01, \*\*\*p < 0.001. Data are expressed as the means  $\pm$  SDs)



**Figure 3**

CircST3GAL6 inhibits tumor growth and metastasis in vivo. a. Overexpression of circST3GAL6 inhibited the growth of xenograft tumors, while knockdown of circST3GAL6 promoted tumor growth. b. The volume and weight of xenograft tumors were measured. c. The tumor tissues were stained with Ki67 antibody, scale bar = 20µm. d. Overexpression of circST3GAL6 inhibited lung metastasis, while knockdown of circST3GAL6 promoted lung metastasis. e. Hematoxylin-eosin staining showed the size of lung metastatic tissues; scale bar = 200 µm. (\*p < 0.05, \*\*p < 0.01, \*\*\*p < 0.001. Data are expressed as the means ± SDs)

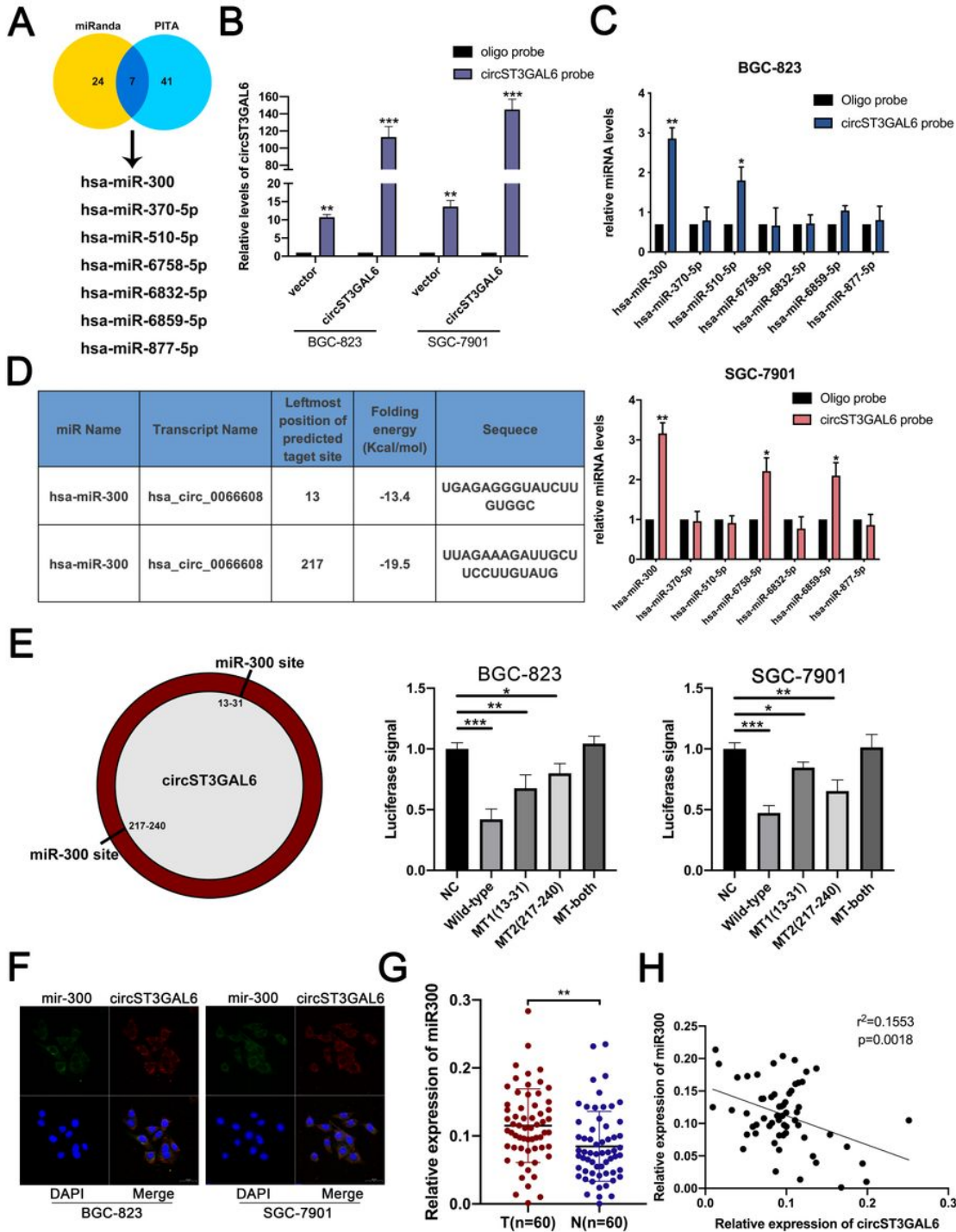


**Figure 4**

CircST3GAL6 functions as a miRNA sponge of miR-300. a. Venn diagram showing the target miRNAs of circST3GAL6 predicted by miRanda and PITA. b. The expression of circST3GAL6 in BGC823 and SGC7901 cell lysates was detected via qRT-PCR. c. qRT-PCR analysis to examine the expression of candidate miRNAs after pull-down assays in BGC-823 and SGC-7901 cells. d. Sequence diagram of the binding sites between circST3GAL6 and miR-300. e. Analysis of luciferase activity in BGC823 and SGC7901 cells transfected with WT or MUT miR-300. f. FISH assay showed that circST3GAL6 and miR-300 were co-localized in the cytoplasm. g. qRT-PCR showed that the expression of miR-300 in GC tissues was significantly higher than that in adjacent normal tissues. h. qRT-PCR showed that the levels of circST3GAL6 and miR-300 were negatively correlated. (\* $p < 0.05$ , \*\* $p < 0.01$ , \*\*\* $p < 0.001$ . Data are expressed as the means  $\pm$  SDs)

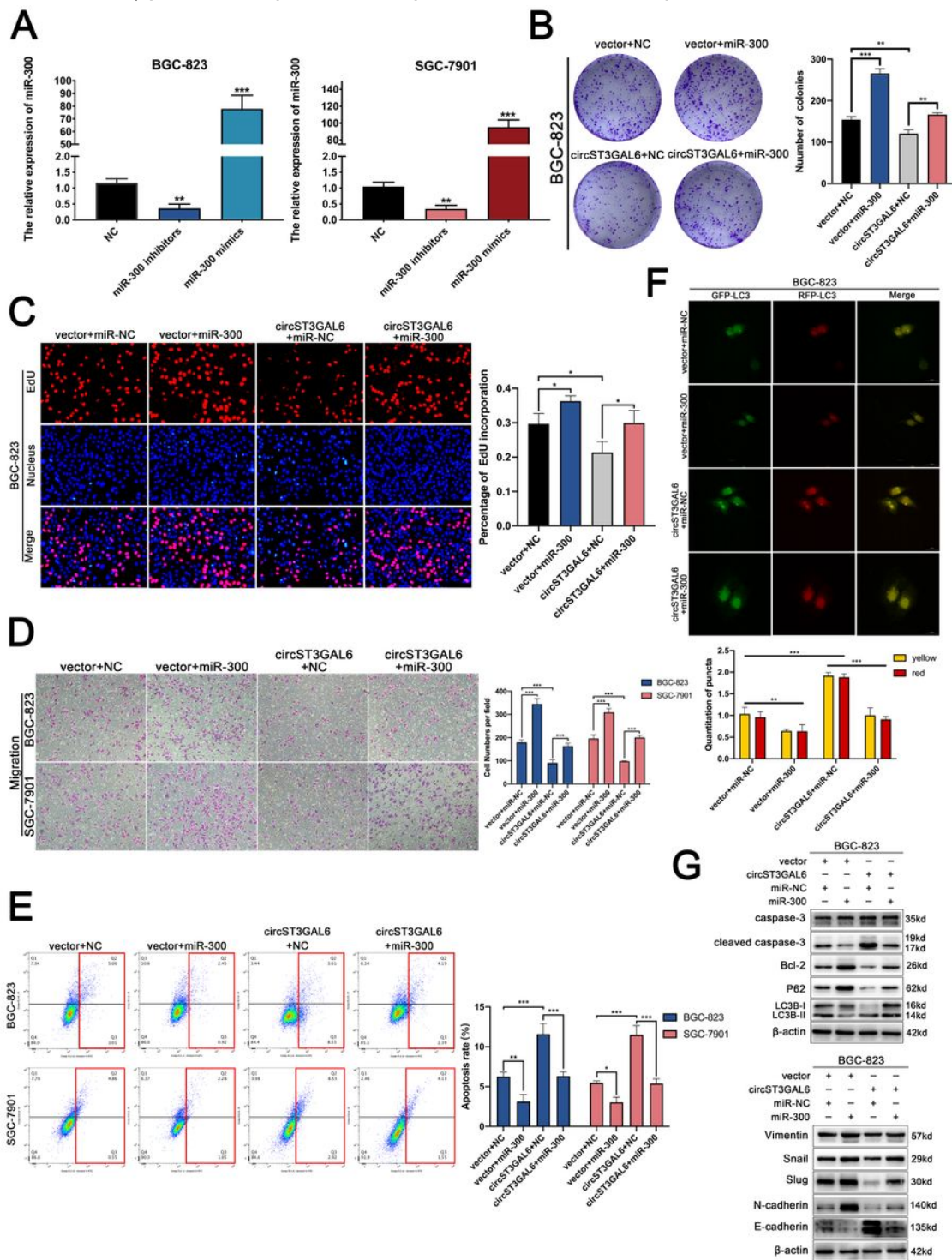


## Figure 5

Overexpression of miR-300 reverses the effect of circST3GAL6 on GC cells. a. The expression levels of miR-300 in BGC-823 and SGC-7901 cells transfected with miR-300 inhibitors or mimics were determined by qRT-PCR. b. and c. miR-300 mimics could restore the effect of circST3GAL6 on cell proliferation in BGC-823 cell by colony formation and EDU assays. d. The inhibition of cell migration by circST3GAL6 overexpression was restored by miR-300 mimics in BGC-823 and SGC-7901 cells. e. The promotion of cell apoptosis by circST3GAL6 overexpression was restored by miR-300 mimics in BGC-823 and SGC-7901 cells. f. The effect of circST3GAL6 overexpression on autophagy can be recovered by miR-300 in BGC-823 cell, scale bar = 20 $\mu$ m. g. Expression levels of apoptotic, EMT and autophagy proteins were examined by western blotting in BGC-823 cell. (\*p < 0.05, \*\*p < 0.01, \*\*\*p < 0.001. Data are expressed as the means  $\pm$  SDs)

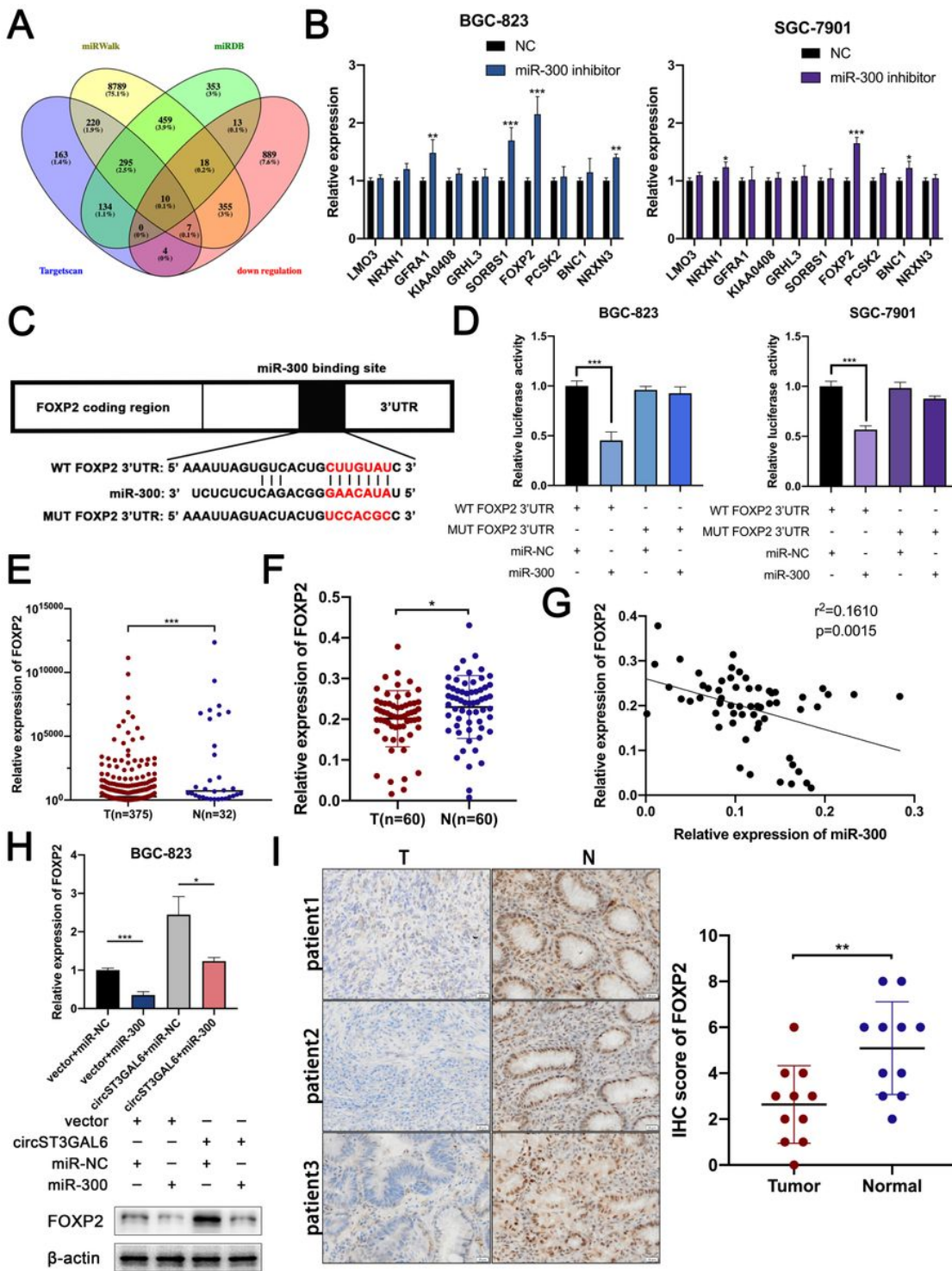


**Figure 6**

FOXP2 is a target of circST3GAL6 by sponging miR-300. a. Venn diagram of target genes of miR-300 predicted by miRWalk, miRDB, TargetScan and down-regulated genes of TCGA. b. qRT-PCR analysis of the relative levels of the 10 candidate genes in BGC-823 and SGC-7901 cells transfected with miR-300 inhibitor or negative control. c. Schematic of potential binding site of miR-300 for FOXP2. d. Luciferase reporter assay for determining whether miR-300 could bind to wt-FOXP2-3'UTR or mut-FOXP2-3'UTR. e. The TCGA database showed that the expression of FOXP2 in GC tissues was significantly lower than that in normal tissues. f. qRT-PCR showed that FOXP2 was significantly lower in GC tissues. g. qRT-PCR showed that the expression levels

of circST3GAL6 and FOXP2 were positively correlated. h. Overexpression of miR-300 could restore the effect of CircST3GAL6 on FOXP2 expression by qRT-PCR and western blotting in BGC-823 cell. i. Immunohistochemistry showed that the expression of FOXP2 was lower in GC tissues than that in adjacent normal tissues; scale bar = 200  $\mu\text{m}$ . (\* $p < 0.05$ , \*\* $p < 0.01$ , \*\*\* $p < 0.001$ . Data are expressed as the means  $\pm$  SDs)

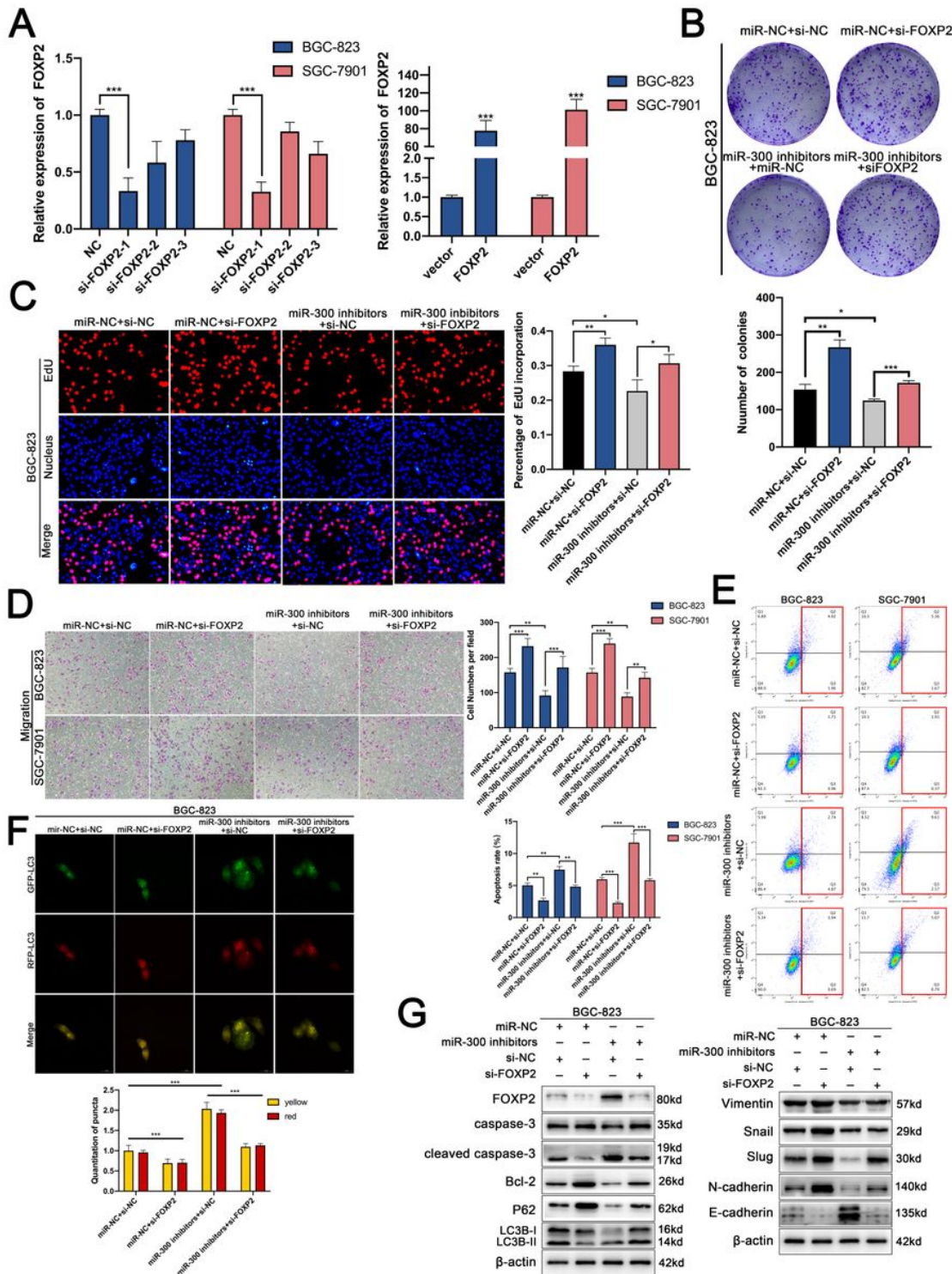


**Figure 7**

Knockdown of FOXP2 reverses the effect of miR-300 inhibitors on GC cells. a. The expression levels of FOXP2 in BGC-823 and SGC-7901 cells transfected with FOXP2 si-RNAs or FOXP2 overexpression plasmid were

determined by qRT-PCR. b. and c. Knockdown of FOXP2 could restore the effect of miR-300 inhibitors on cell proliferation in BGC-823 cell by colony formation and EDU assays. d. The inhibition of cell migration by miR-300 inhibitors was restored by knockdown of FOXP2 in BGC-823 and SGC-7901 cells. e. The promotion of cell apoptosis by miR-300 inhibitors was restored by knockdown of FOXP2 in BGC-823 and SGC-7901 cells. f. The effect of miR-300 inhibitors on autophagy can be recovered by knockdown of FOXP2 in BGC-823 cell, scale bar = 20 $\mu$ m. g. Expression levels of apoptotic, EMT and autophagy proteins were examined by western blotting in BGC-823 cell. (\* $p < 0.05$ , \*\* $p < 0.01$ , \*\*\* $p < 0.001$ . Data are expressed as the means  $\pm$  SDs)

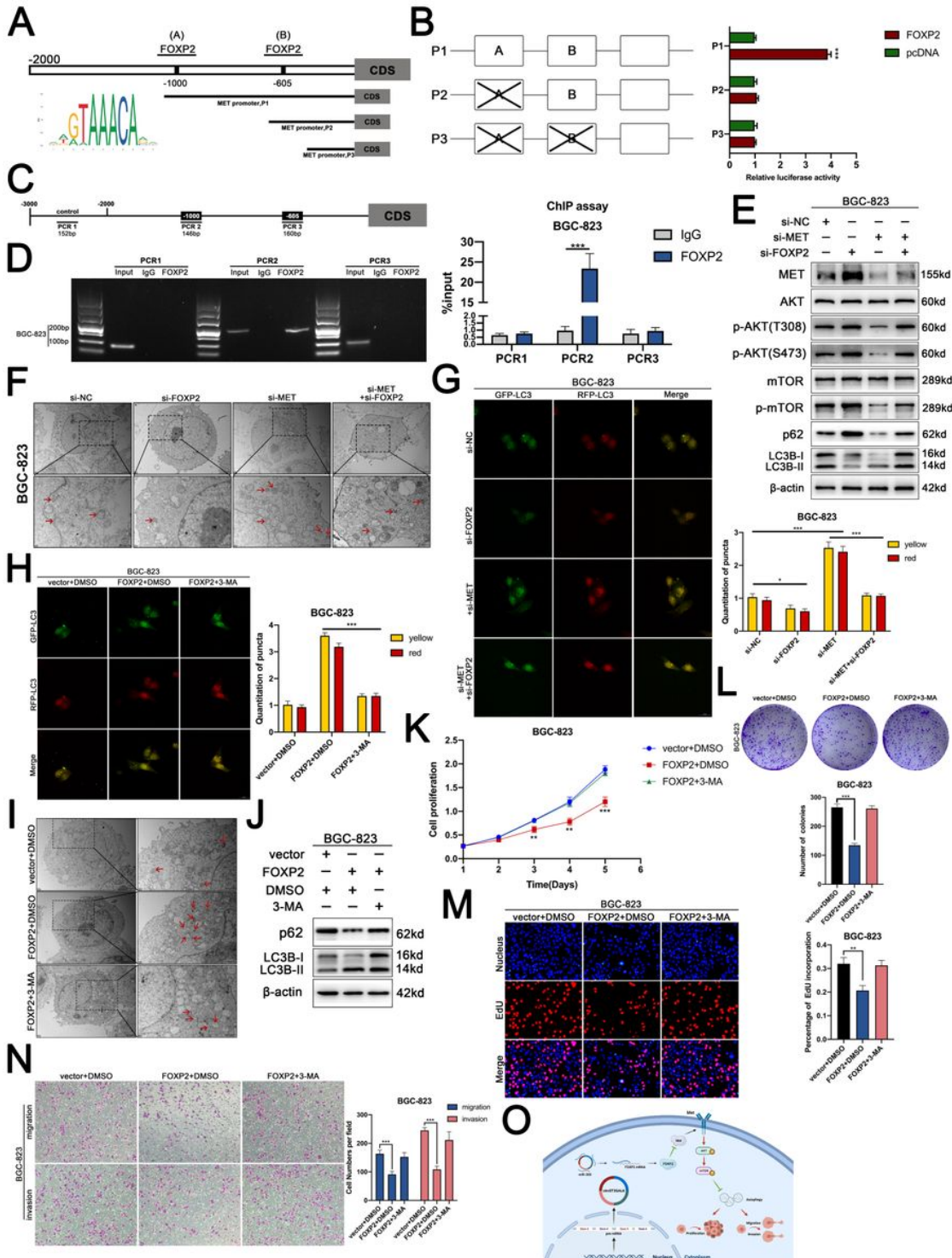


Figure 8

FOXP2 transcriptionally inhibits MET and regulates autophagy through AKT/mTOR axis which regulates the malignant progression of GC cells. a. Schematic diagram showed three luciferase reporters cover different DNA sequences of MET promoter region. b. Luciferase reporter assay analysis of three MET promoter luciferase reporters in BGC-823 cells transfected with FOXP2 or pcDNA. c. Schematic diagram showed three primers for CHIP assay. d. qRT-PCR was performed in BGC-823 cell after pulling down FOXP2 using three pairs of primers to investigate the potential FOXP2 binding sites in MET promoter region. e. Expression levels of FOXP2, MET/AKT/mTOR and autophagy proteins were examined by western blotting. f. and g. The effect of overexpression of circST3GAL6 on autophagy can be recovered by knockdown of FOXP2 via confocal microscopy (scale bar = 20 $\mu$ m) and transmission electron microscopy scale bar = 1 $\mu$ m in BGC-823 cell. h. and i. The effect of overexpression of FOXP2 on autophagy can be recovered by 3-MA (5nM, 24 h) via confocal microscopy (scale bar = 20 $\mu$ m) and transmission electron microscopy (scale bar = 1 $\mu$ m) in BGC-823 cell. j. Expression levels of autophagy-related proteins were examined by western blotting in BGC-823 cell. k.-m. 3-MA (5nM, 24 h) could restore the effect of FOXP2 overexpression on cell proliferation in BGC-823 cell by CCK8, colony formation and EdU assays. n. 3-MA (5nM, 24 h) could restore the effect of FOXP2 overexpression on cell migration and invasion in BGC-823 cell transwell assays. o. CircST3GAL6 mechanism diagram. (\*p < 0.05, \*\*p < 0.01, \*\*\*p < 0.001. Data are expressed as the means  $\pm$  SDs)

## Supplementary Files

This is a list of supplementary files associated with this preprint. Click to download.

- [FigS2.jpg](#)
- [FigS3.jpg](#)
- [FigS4.jpg](#)
- [FigS1.jpg](#)
- [FigS5.jpg](#)